journal

J. Am. Ceram. Soc., 78 [12] 3195–200 (1995)

Simulation of Segregation to Free Surfaces in Cubic Oxides

Corbett C. Battaile, Reza Najafabadi,*,† and David J. Srolovitz

Department of Materials Science and Engineering, University of Michigan, Ann Arbor, Michigan 48109

Segregation of isovalent solute cations to (001) and (011) free surfaces in cubic metal oxides is investigated using atomistic computer simulations. Solute concentrations are represented by a mean-field approximation, and equilibrium distributions of solute are calculated by minimizing the free energy. Surface energy effects are found to dominate segregation behavior, even when in competition with misfit strain energy effects. Results are compared with a conventional Langmuir–McLean (LM) analysis. The two approaches are found to agree well in certain cases, but the LM treatment fails to reproduce important phenomena revealed using the free energy method (i.e., segregation to subsurface atomic layers).

I. Introduction

THE properties of many solids depend strongly upon segregation to interfaces. For example, segregation to grain boundaries can affect strength[1,2] and conductivity[2]; and segregation to free surfaces plays an important role during sintering, catalysis, and film deposition.[3]

Although many factors control segregation, simple and convenient models are often satisfactory to predict segregation behavior. However, such models are usually empirical and/or contain simplifying assumptions that can make their reliability suspect. For example, segregation is often assumed to depend primarily on solute misfit. This effect has been used[4] to explain surface segregation in metal oxides. However, misfit effects are often of secondary importance compared to surface energy effects, as demonstrated[5] for binary metallic alloys.

The Langmuir–McLean (LM) theory provides a convenient model of segregation in ideal systems. In some cases, this theory provides an adequate prediction of segregation behavior. However, the enthalpy of segregation, upon which the LM analysis is based, can depend strongly on the surface concentration in ionic solids.[6] This dependence is neglected by the basic LM treatment.

In addition, most common applications of the LM model yield only a single surface concentration value. When derived from experimental measurements, this concentration value corresponds to an average over several atomic planes at the surface. On the other hand, the surface concentration obtained through simulations using the LM theory usually represents the concentration of the surface layer only. Many atomistic simulations have found that segregation can be appreciable over several atomic planes. This finite extent of the segregation is neglected in LM-based simulations and beyond the resolution of most experimental probes.

Since measurements of concentration on an atomic scale are difficult to make, experimental data are scarce. Further, the existing experimental data base is often inconsistent because different experimental techniques measure segregation with different resolution. This hinders experimental verification of these simple models. Therefore, simulation techniques provide a valuable tool, not only to help us understand segregation phenomena, but also to predict segregation behavior as a complement to or in lieu of experiment.

There are several methods for simulating segregation in solids. Perhaps the most common (and accurate) are Monte Carlo techniques, which have been successfully applied[5,7] to study segregation in metals. However, these methods are computationally demanding, and have not yet been applied to study segregation in ionic solids.

Alternatively, free energy minimization (FEM) methods,[8,9] though not as accurate as Monte Carlo schemes, are computationally efficient and allow convenient access to thermodynamic information. These techniques have been successfully applied to study segregation in metals, and have been shown[10–12] to agree well with Monte Carlo predictions in these materials. Our preliminary results[13] using Monte Carlo techniques to study segregation in ionic systems show an excellent correspondence with FEM data.

Although several previous computational studies[4,6,14,15] of segregation in ionic solids have employed LM-like analyses to predict segregation to interfaces, in the present paper we report segregation results for ionic solids based upon a more comprehensive treatment. This treatment employs the FEM method, which combines conventional interionic pair potentials with a local harmonic[8] approximation of lattice dynamics and a mean-field effective atom[10] representation of solute concentrations. We apply the FEM method to examine surface segregation in several cubic metal oxides in order to examine the validity of some of the simpler treatments and assumptions discussed above. Since this method is based upon the minimization of free energy, it predicts *equilibrium* free-surface segregation behavior and, hence, provides a tool for understanding and predicting segregation behavior.

II. Methods

(1) Interionic Potential

The energetics and structures of ionic materials have been investigated computationally for many years.[16–21] For most applications, pair potentials (parameterized either empirically using experimental data or analytically from quantum-mechanical calculations) accurately predict the properties of ionic crystals.

The potential energy, U, is of the Born–Mayer form, i.e., a pairwise sum over all bonds,

$$U = \sum_{i=1}^{N} \sum_{j>i} \left[B_{ij} \exp(-b_{ij} r_{ij}) - \frac{C_{ij}}{r_{ij}^6} + \frac{q_i q_j}{r_{ij}} \right] = \sum_{i=1}^{N} \sum_{j>i} \Phi_{ij} \quad (1)$$

where the summation over ions j includes the neighbors of ion i; N is the total number of ions; B_{ij}, b_{ij}, and C_{ij} are parameters describing the short-range interaction between ions i and j; r_{ij} is the separation between ions i and j; q_i is the charge on ion i; and Φ_{ij} is the bond energy between ions i and j. The first term in the summation represents an exponential repulsive interaction; the

Y.-M. Chiang—contributing editor

Manuscript No. 192832. Received February 14, 1995; approved June 27, 1995.

Supported by the Advanced Research Projects Agency and the Office of Naval Research under Grant No. N00014-91-J-4019.

*Member, American Ceramic Society.

†Currrent address: Knolls Atomic Power Laboratory, Schenectady, New York 12309.

second, a van der Waals attractive interaction; and the third, a long-range Coulombic interaction.

The difficulties associated with summation of the Coulomb energy are handled using Ewald's method.[22,23] Ionic polarization is included via the shell model,[24] which considers each ion as a charged core and a charged, massless, spherical shell. The charges of the core and shell are chosen such that the sum yields the total ionic charge. The core and shell are connected by a harmonic spring having a force constant, k. Short-range interactions are only between shells, but the Coulombic interactions exist between all cores and shells (except between the core and shell of the same ion). Therefore, within the framework of the shell model, a system containing N ions contains $2N$ interacting bodies (N cores and N shells).

(2) Free Energy

The equilibrium configuration of an ionic solid at finite temperature can be obtained by minimizing the Helmholtz free energy. This free energy, A, is a sum of the potential energy, U; a vibrational energy, A_v, which includes kinetic energy and vibrational entropy; and a contribution from the configurational entropy, S_c,

$$A = U + A_v - TS_c \tag{2}$$

where T is the temperature.

The vibrational energy of a system of N harmonic oscillators in three dimensions can be expressed in terms of the $3N$ normal-mode vibrational frequencies of the system. In the classical limit, this energy is

$$A_v = k_B T \sum_{n=1}^{3N} \ln\left(\frac{\hbar\omega_n}{k_B T}\right) \tag{3}$$

where ω_n is the nth normal-mode vibrational frequency, k_B is Boltzmann's constant, and $\hbar$ is Planck's constant.

In a system of harmonic oscillators, the normal-mode vibrational frequencies, ω_n, are related to the system's dynamical matrix, $\mathbf{D}$, by

$$(\omega_n)^2 \mathbf{M}\vec{u} = \mathbf{D}\vec{u} \qquad (n = 1, 2, \ldots, 3N) \tag{4}$$

where $\mathbf{M}$ is a diagonal matrix containing the square roots of the products of the oscillator masses, and $\vec{u}$ is a vector containing the displacements of the oscillators. The dynamical matrix is the Hessian of the potential energy, i.e., the second derivatives of the potential energy with respect to the positions of the oscillators evaluated at the mean positions. Because each ion consists of two oscillators (a core and a shell), the matrix, $\mathbf{D}$, is $6N \times 6N$. Since the shells are assumed massless, Eq. (4) can be rewritten as a $3N \times 3N$ system. (See Ref. 18 for a detailed discussion of shell model lattice dynamics in ionic crystals.)

In the current work, each ion is assumed to vibrate as a rigid (though polarizable) object, i.e., a shell which is rigidly attached to (but not necessarily centered at) the core. This assumption makes analytic derivation of the vibrational forces tractable, and is reasonable because the shell model springs are relatively stiff (i.e., k is large) and the vibrational energy contributes little to segregation behavior. Nonetheless, despite this simplifying assumption in the calculation of vibrational energies, the potential energy fully incorporates the shell model.

To further facilitate calculation of equilibrium properties, the vibrational energy is approximated using the local harmonic[8] model. This model treats a solid as a system of harmonic oscillators in which the vibrations of an atom are not coupled to the vibrations of the other atoms. The resulting vibrational energy is a function of the three local vibrational frequencies of each of the N oscillators. Therefore, the vibration of each ion is described by a 3×3 local dynamical matrix, $\mathbf{D}_i$, which corresponds to a submatrix on the diagonal of $\mathbf{D}$. Since each ion is assumed to consist of only one oscillator (core + shell), the N local dynamical matrices consist of sums of the second derivatives of the potential energy with respect to the ion positions,

$$D_i^{(\alpha\beta)} = \frac{\partial^2 U}{\partial r_i^{(c\alpha)}\,\partial r_i^{(c\beta)}} + \frac{\partial^2 U}{\partial r_i^{(c\alpha)}\,\partial r_i^{(s\beta)}} + \frac{\partial^2 U}{\partial r_i^{(s\alpha)}\,\partial r_i^{(c\beta)}} + \frac{\partial^2 U}{\partial r_i^{(s\alpha)}\,\partial r_i^{(s\beta)}} \tag{5}$$

where $D_i^{(\alpha\beta)}$ is an element of the 3×3 local dynamical matrix of ion i coupling the vibrations of that ion in the α and β directions; the first superscript on r_i denotes the core (c) or shell (s) of ion i; and the second superscript on r_i denotes one of the directions. The second derivatives in Eq. (5) are evaluated at the mean positions of the ion cores and shells. (Again, the core and shell need not be concentric.)

The local harmonic approximation has performed well when applied[10–12] to defect energy calculations in metals. Unfortunately, in many ionic solids the vibrations of two different atoms are strongly coupled compared to two vibrations of the same atom (since the Coulomb potential obeys the Laplace equation,[25] and the coordination is relatively low). Therefore, the local approximation is less accurate in ionic systems than in metals for determining defect energies.[26] However, segregation behavior is much less sensitive to the vibrational energy than are defect energies. In any case, the local harmonic model is an improvement over zero-temperature calculations for this purpose. Alternative methods for obtaining vibrational energies and forces within the quasi-harmonic approximation are currently being investigated, and will be reported in a future paper.

(3) Langmuir–McLean Theory

Many earlier simulations[4,6,14,15] of segregation to surfaces in ionic solids have combined calculated data with the LM theory to determine the segregant. This approach is generally valid only in the ideal limit, wherein bulk solute concentrations are small, segregation is weak, and interactions between solute atoms are negligible.

The method is formulated in terms of the enthalpy of segregation, ΔH,

$$\Delta H = \Delta U^{(S)} - \Delta U^{(B)} \tag{6}$$

where $\Delta U^{(S)}$ is the zero-temperature formation energy of a solute atom at the surface, and $\Delta U^{(B)}$ is that in the bulk. If vibrational effects are negligible and ΔH is constant, then a simple analysis yields an Arrhenius relation between the concentration of the solute at the surface, $c^{(S)}$, and that in the bulk, $c^{(B)}$,

$$\frac{c^{(S)}}{1 - c^{(S)}} = \frac{c^{(B)}}{1 - c^{(B)}} \exp\left(-\frac{\Delta H}{k_B T}\right) \tag{7}$$

This expression can be used very conveniently to calculate equilibrium solute concentrations at surfaces (or at any other crystallographic feature) provided ΔH is known and is constant. However, this analysis neither accounts for, nor provides any information about, solute distributions elsewhere in the crystal. This and other key assumptions inherent in LM theory limit its utility.

(4) Effective Atom Method

In this work, we employ the concept of an effective atom[10] to investigate segregation to surfaces in ionic solids. To visualize this method, imagine a crystal containing some concentration of solute, A, in a solvent, B. During a given time, a lattice site will be occupied by solute atoms with a certain probability $c^{(A)}$ and by solvent atoms with a probability $c^{(B)} = 1 - c^{(A)}$. One can think of these probabilities as time-averaged site concentrations, and neglecting temporal correlation between these concentrations, one can define the average spatial solute concentration profile, $c_i^{(A)}$, at each site, i. Within this mean-field approximation, the average bond energy between ions i and j, Φ_{ij}, can be written as

$$\Phi_{ij} = c_i^{(A)} c_j^{(A)} \Phi_{ij}^{(AA)} + c_i^{(B)} c_j^{(B)} \Phi_{ij}^{(BB)} + [c_i^{(A)} c_j^{(B)} + c_i^{(B)} c_j^{(A)}] \Phi_{ij}^{(AB)} \tag{8}$$

where the first superscript on Φ_{ij} denotes the species (A or B) of ion i, and the second superscript on Φ_{ij} denotes the species of ion j. This approximation is simply a mean-field representation of the concentration in a solid solution. (Notice that, although this method contains certain assumptions that neglect correlations between site concentrations, it explicitly includes the effects of the interaction between solute atoms.)

The same averaging scheme is applied to the second derivatives in Eq. (5) to obtain the N local dynamical matrices, from which the $3N$ local vibrational frequencies are calculated. Similarly, the mass of the ion at site i is

$$m_i = c_i^{(A)} m^{(A)} + c_i^{(B)} m^{(B)} \tag{9}$$

where m_i is the effective mass of ion i, $m^{(A)}$ is the mass of species A, and $m^{(B)}$ is the mass of species B. The effective shell model spring constant of ion i is calculated similarly, with the mass, m, in Eq. (9) replaced by the spring constant, k.

Since the site concentrations are assumed to be uncorrelated, the configurational entropy, S_c, can be expressed using a simple point approximation,

$$S_c = -k_B \sum_{i=1}^{N} \{c_i^{(A)} \ln [c_i^{(A)}] + c_i^{(B)} \ln [c_i^{(B)}]\} \tag{10}$$

In order to study segregation, it is convenient to consider a reduced grand canonical ensemble wherein the total number of the ions remains fixed and the relative amounts of each species are allowed to vary. The appropriate free energy to characterize this ensemble is the reduced grand potential, Ω,

$$\Omega = A + \Delta\mu \sum_{i=1}^{N} c_i^{(A)} \tag{11}$$

where $\Delta\mu$ is the difference between the chemical potentials of the solute and solvent species in the bulk environment. $\Delta\mu$ is determined from

$$\Delta\mu = \frac{\partial A_{\text{bulk}}}{\partial c_i^{(A)}} \tag{12}$$

where A_{bulk} is the free energy of the bulk crystal with each site concentration set to the desired value. This chemical potential difference is kept constant, which ensures that the bulk maintains the predetermined concentration.

Using the model outlined above, equilibrium time-averaged concentration profiles are predicted by minimizing the reduced grand potential, Ω, with respect to ion positions (i.e., cores and shells independently) and site concentrations. This method has been successfully applied to study segregation[10,11] and vacancy formation energies[12] in metallic alloys, and a similar approach was used[27] to accurately calculate bulk properties of alkali halide solid solutions.

III. Results

Using the method described above, equilibrium concentration profiles at interfaces are determined for selected cubic metal oxides doped with isovalent cation species. For the purposes of the present study, substitution of isovalent cations onto the cation sublattice in cubic metal oxides is considered, and substitution of these isovalent cations onto the anion (oxygen) sublattice is prohibited. Segregation to (001) and (011) free surfaces is examined.

The interionic potential parameters are taken from Ref. 28 and reproduced in Table I. Only the shell charges are given, since the core charge can be obtained by subtracting the shell charge from the total ionic charge (i.e., ± 2). Short-range interactions between cations are neglected by these potentials, and therefore doped systems (e.g., MgO doped with Ca^{2+}, denoted $(Ca_xMg_{1-x})O$) can be described using the potential parameters for the corresponding oxides (e.g., MgO and CaO), assuming transferability of the O–O potential. Van der Waals interaction is allowed between anions only.

The simulations are performed using a rectangular supercell of dimension $1 \times 1 \times 9$ conventional unit cells (72 ions) having the sodium chloride structure in the desired orientation. Periodic boundary conditions are imposed in all three directions. The initial configuration corresponds to the equilibrium lattice parameter of the defect-free crystal at the temperature of interest with all site concentrations set to the desired bulk value. The chemical potential difference, $\Delta\mu$, is calculated using this configuration. To simulate free surfaces, the repeat length in the z-direction is increased by 40 times the nearest-neighbor distance. In this way, we simulate an infinite array of slabs, each having two free surfaces, separated by a vacuum. Finally, the lengths of the simulation cell in the x and y directions are fixed (yielding a constant surface area ensemble) and the reduced grand potential, Ω, is minimized with respect to the ion positions and the cation site concentrations using the Polak–Ribiere conjugate-gradient algorithm.[29] Equilibrium concentration profiles in the relaxed systems are thereby calculated. Segregation behavior has also been determined for simulation cells of dimension $2 \times 2 \times 7$ unit cells (224 ions) using the same approach, and the results do not significantly differ from those obtained using the smaller simulation cell size.

For comparison, a similar procedure is employed to predict segregation using the LM theory. For this purpose, a simulation cell of dimension $2 \times 2 \times 7$ unit cells (224 ions) is used. The initial configuration is determined as above, but for a pure oxide system. A cation in the center (bulk) of the supercell is replaced by the desired cation solute. The energy of the system at zero temperature is then minimized with respect to the ion positions and the resulting formation energy, $\Delta U^{(B)}$, is calculated. A similar procedure is used to obtain the formation energy, $\Delta U^{(S)}$, of the solute at the free surface. The two formation energies are used to calculate the enthalpy of segregation, $\Delta H = \Delta U^{(S)} - \Delta U^{(B)}$, which is used to obtain the desired surface concentration according to Eq. (7).

All concentration values are given in atomic fractions. Because only substitution onto the cation sublattice is considered, concentrations correspond to the fraction of *cation* sites occupied by solute atoms.

Figure 1 contains calculated equilibrium solute concentrations at (001) and (011) free surfaces as functions of the bulk concentration in $(Co_xNi_{1-x})O$ at $T = 600$ K and $(Fe_xMn_{1-x})O$ at $T = 1000$ K. Co^{2+} is found to segregate to the (001) and (011) surfaces of $(Co_xNi_{1-x})O$ for all bulk Co^{2+} concentrations (Figs. 1(a) and (b)). Segregation of Co^{2+} to the (011) surface is slightly stronger than to the (001) surface in this system. Mn^{2+} is found to segregate to both surfaces in $(Fe_xMn_{1-x})O$ (Figs. 1(c) and (d)). Segregation to the (011) surface in $(Fe_xMn_{1-x})O$ is slightly stronger than to the (001) surface.

Surface solute concentrations obtained using the LM treatment are also shown in Fig. 1 for the (001) and (011) surfaces in $(Co_xNi_{1-x})O$ and $(Fe_xMn_{1-x})O$. Two LM results are shown for each case, since the heat of segregation may be determined at either end of the phase diagram. For example, the LM analysis of the CoO–NiO system can be performed by considering either Co^{2+} in NiO (which is appropriate for low bulk Co^{2+} concentrations) or Ni^{2+} in CoO (appropriate for high bulk Co^{2+} concentrations). The LM calculations agree fairly well with FEM in both systems. The LM theory neglects the effects of atomic vibration, and these results suggest that vibrational effects are of secondary importance in determining segregation in these materials.

Concentration profiles near the (001) and (011) surfaces are shown for $(Ni_{0.3}Co_{0.7})O$ and $(Fe_{0.1}Mn_{0.9})O$ at $T = 600$ K in Fig. 2. (Note that the (001) interplanar spacing is not equal to the (011) interplanar spacing.) In these two examples, the solvent cation segregates to the free surface. Considerable segregation of solute to subsurface atomic layers is seen near (001) and especially (011) surfaces in both systems.

Table I. Interionic Potential Parameters for Selected Oxides†

Ion	$q^{(s)}$ (e)	k (eV·Å^{-2})	Bond	B (eV)	b (Å^{-1})	C (eV·Å^6)
O^{2-}	−2.8107	46.1309	O–O	22764.3	6.7114	−20.37
Ca^{2+}	3.467	113.8729	Ca–O	1179.3	2.9403	
Co^{2+}	4.933	229.1770	Co–O	1942.0	3.5149	
Fe^{2+}	3.372	81.4583	Fe–O	1249.1	3.2478	
Mn^{2+}	3.928	123.2264	Mn–O	1052.8	3.0779	
Ni^{2+}	4.342	170.4199	Ni–O	1914.9	3.5753	
Sr^{2+}	3.350	63.2492	Sr–O	950.1	2.6767	

†After Sangster and Stoneham.[28] $q^{(s)}$ is the charge on the shell; k is the shell model spring constant; and B, b, and C are short-range interaction parameters.

IV. Discussion

(1) *Misfit Strain and Surface Energy Effects*

A substitutional solute atom that is different in size from the solvent might be expected to segregate to a free surface to minimize the strain energy. This is often observed, and has been used to explain previous computational results for ionic solids.[4] However, segregation to a free surface is also accompanied by some change in surface energy.[5] Strain and surface energy effects can compete to determine the magnitude and sign of the segregation. In many of the examples shown here, segregation behavior contradicts what one might expect based on misfit strain arguments. In these cases, segregation is apparently dominated by surface energy effects.

Consider the (001) surface of $(Fe_{0.1}Mn_{0.9})O$ at T = 600 K (Fig. 2(b)). The ionic radius[30] of the Mn^{2+} cation is $r_{Mn^{2+}}$ = 0.67 Å and that of Fe^{2+} is $r_{Fe^{2+}}$ = 0.77 Å. Nevertheless, the solvent cation (Mn^{2+}) segregates to the surface in this system. At a bulk

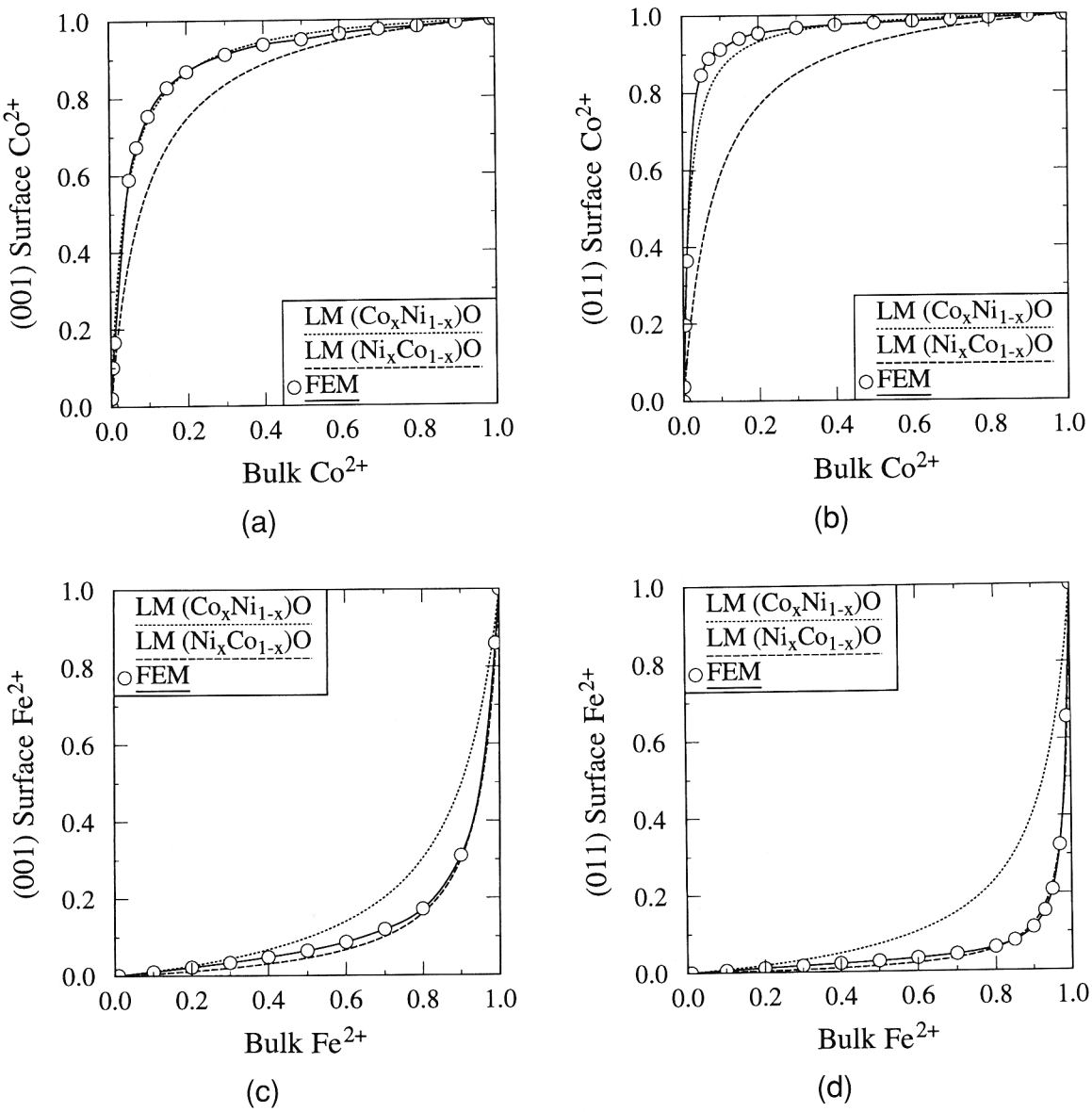

Fig. 1. Free energy minimization (FEM) predictions of equilibrium solute concentrations at free surfaces, shown as functions of bulk concentrations for the (a) (001) surface of $(Co_xNi_{1-x})O$ at T = 600 K, (b) (011) surface of $(Co_xNi_{1-x})O$ at T = 600 K, (c) (001) surface of $(Fe_xMn_{1-x})O$ at T = 1000 K, and (d) (011) surface of $(Fe_xMn_{1-x})O$ at T = 1000 K. Langmuir–McLean (LM) results are provided for comparison.

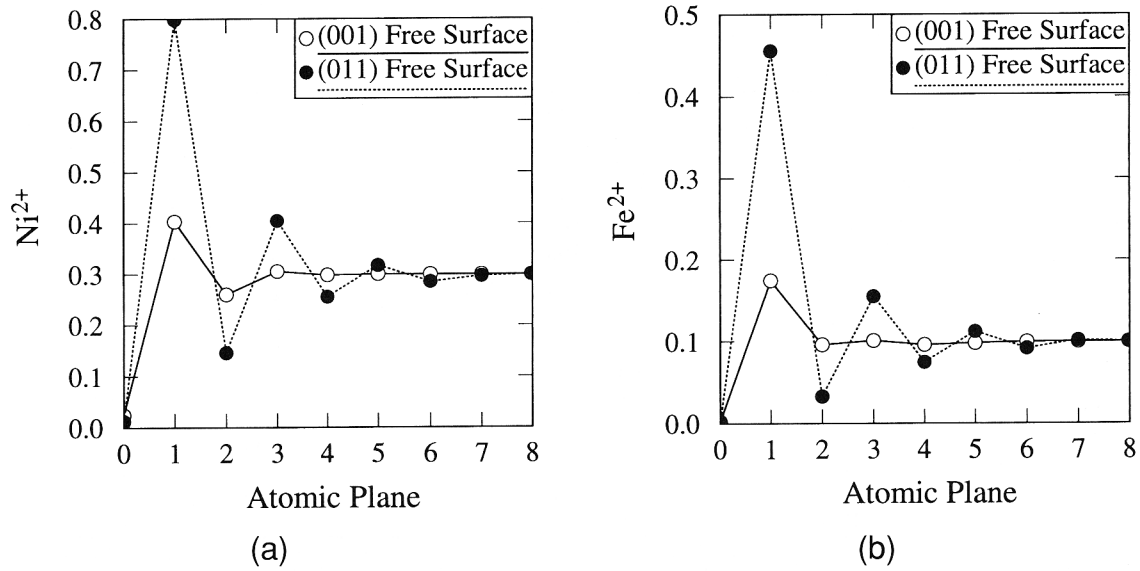

Fig. 2. Equilibrium solute concentration profiles at $T = 600$ K near the (001) and (011) surfaces of (a) $(Ni_{0.3}Co_{0.7})O$ and (b) $(Fe_{0.1}Mn_{0.9})O$.

Fe^{2+} concentration of 0.1, where Fe^{2+} is the minority cation species, misfit strain arguments suggest that Fe^{2+} would segregate to the free surface. However, this behavior is not observed. The reason that Mn^{2+} segregates in this case can be found by examining the relative (001) surface energies of the oxides, MnO and FeO. (Recall that the interionic potentials used in this study neglect short-range cation–cation interaction.) The surface energies of the two oxides should be calculated in a crystal environment corresponding to the equilibrium configuration of the $(Fe_{0.1}Mn_{0.9})O$ surface at $T = 600$ K. This is difficult to do, since many factors contribute to the surface energy of a solid solution. For the purpose of an unambiguous comparison, we simply dilate the unrelaxed MnO and FeO surfaces to the equilibrium volume associated with the $(Fe_{0.1}Mn_{0.9})O$ solid solution at $T = 600$ K and evaluate the surface energy at zero temperature. In this way, we avoid the introduction of surface relaxation which, though appropriate for the individual oxide systems, may not be meaningful when applied to $(Fe_{0.1}Mn_{0.9})O$. Assuming that the primary contribution to the change in surface energy is through broken bonds at the surface, this is a reasonable approach. (The surface energies of MnO and FeO are sufficiently different that such a comparison is certainly valid in this case.) The unrelaxed (001) surface energy of MnO, $\gamma^*_{(001)} = 990$ erg/cm^2, calculated for a lattice parameter of $a = 4.469$ Å, is substantially lower than that of FeO, $\gamma^*_{(001)} = 1337$ erg/cm^2. Therefore, even though Fe^{2+} is expected to segregate to the free surface to minimize strain energy, Mn^{2+} segregates in these simulations to minimize surface energy. (In cases such as this, where the surface energies of the oxide components significantly differ, a valid comparison can be made using the fully relaxed surface energies, which are $\gamma_{(001)} = 843$ erg/cm^2 for MnO and $\gamma_{(001)} = 997$ erg/cm^2 for FeO.)

In almost every case where strain and surface energy effects are in competition to determine the segregating species, surface energy effects dominate in these simulations. Some examples are provided in Table II. This phenomenon is not very surprising in these systems, since isovalent cations are similar in size, and misfit strain energies are small compared with surface energy differences. This can be verified by a simple calculation. Friedel[31] proposed an expression for the elastic energy, E_{elastic}, of a misfitting solute,

$$E_{\text{elastic}} = \frac{24\pi K^{(A)} G^{(B)} (r^{(B)})^3 r^{(A)} \left(\frac{r^{(A)}}{r^{(B)}} - 1\right)^2}{3K^{(A)} r^{(A)} + 4G^{(B)} r^{(B)}} \qquad (13)$$

where $K^{(A)}$ is the bulk modulus of the solute, $G^{(B)}$ is the shear modulus of the solvent, and $r^{(A)}$ and $r^{(B)}$ are the radii of the solute and solvent atoms, respectively. Assuming that all of this elastic energy is relieved when a solute atom segregates to a free surface, and that the primary contribution to the surface energy is broken bonds, one can obtain a rough comparison between the misfit and surface energy effects discussed above by comparing E_{elastic} with the difference between the bond energies (which are approximately the cohesive energies divided by 6) of the solute and solvent oxides. Such a comparison is given in Table II for several cases. (See Ref. 28 for the cohesive energies and elastic constants of the oxides.)

These data suggest that the change in misfit strain energy that is associated with the segregation of a solute to a free surface is significantly smaller than the corresponding change in surface energy in all cases except $(Ni_{0.001}Sr_{0.999})O$ (wherein the difference between the cation radii is largest). Since only a fraction of this elastic energy is relieved when a solute atom segregates to a free surface, it is not surprising (based on this comparison) that surface energy effects dominate misfit strain effects to determine segregation in all of the cases presented in Table II.

(2) Concentration Profiles

The effective atom treatment of a solid solution provides information about concentration profiles throughout the system. This information is especially important when studying complicated defects (e.g., grain boundaries and surface steps), but can also reveal important features of segregation to flat free surfaces.

As indicated above, a simple LM analysis can satisfactorily predict concentrations at free surfaces. If segregation is limited to the surface layer, then the LM result might suffice. However, significant segregation to the subsurface atomic layers is observed in these simulations.

Figure 2(a) shows the segregation profile in $(Ni_{0.3}Co_{0.7})O$ at $T = 600$ K. Even though the LM calculation is able to satisfactorily predict the Co^{2+} concentration at the surface of $(Co_xNi_{1-x})O$ (see Fig. 1(a)), the same analysis cannot provide information about the substantial subsurface segregation observed in Fig. 2(b). This subsurface segregation is also seen in $(Fe_{0.1}Mn_{0.9})O$ at $T = 600$ K (Fig. 2(b)). The oscillatory concentration profiles in $(Ni_{0.3}Co_{0.7})O$ and $(Fe_{0.1}Mn_{0.9})O$ might suggest some propensity for ordering (either at the surface or in the bulk). However, no bulk or surface phase transitions are predicted by these simulation methods in $(Ni_{0.3}Co_{0.7})O$ or $(Fe_{0.1}Mn_{0.9})O$ at $T = 600$ K. Therefore, if there is no tendency toward ordering, the subsurface segregation will be driven by a reduction of misfit strain energy, since this is the only other likely candidate. Segregation to the surface in these systems is

Table II. Segregation to (001) and (011) Free Surfaces at $T = 2000$ K†

Solution	a (Å)	r (Å)	Segregant to (001)	$\gamma^*_{(001)}$ (erg·cm^2)	$\gamma_{(001)}$ (erg·cm^2)	Segregant to (011)	$\gamma^*_{(011)}$ (erg·cm^{-2})	$\gamma_{(011)}$ (erg·cm^{-2})	$E_{elastic}$ (eV)	ΔE_{bond} (eV)
$(Co_{0.001}Ca_{0.999})O$	4.913	Ca^{2+}: 1.00 Co^{2+}: 0.74	Ca^{2+}	CaO: 903 CoO: 1606	752 1101	Ca^{2+}	CaO: 2358 CoO: 3339	1884 2604	0.49	0.83
$(Fe_{0.001}Ca_{0.999})O$	4.913	Ca^{2+}: 1.00 Fe^{2+}: 0.77	Ca^{2+}	CaO: 903 FeO: 1493	752 997	Ca^{2+}	CaO: 2358 FeO: 3181	1884 3087	0.23	0.68
$(Ni_{0.001}Ca_{0.999})O$	4.913	Ca^{2+}: 1.00 Ni^{2+}: 0.69	Ca^{2+}	CaO: 903 NiO: 1675	752 1188	Ca^{2+}	CaO: 2358 NiO: 3437	1884 2809	0.69	0.98
$(Co_{0.1}Mn_{0.9})O$	4.517	Mn^{2+}: 0.67 Co^{2+}: 0.74	Mn^{2+}	MnO: 1064 CoO: 1586	843 1101	Mn^{2+}	MnO: 2894 CoO: 3615	2077 2604	0.03	0.38
$(Fe_{0.1}Mn_{0.9})O$	4.522	Mn^{2+}: 0.67 Fe^{2+}: 0.77	Mn^{2+}	MnO: 1070 FeO: 1387	843 997	Mn^{2+}	MnO: 2899 FeO: 3336	2077 3087	0.04	0.23
$(Ni_{0.1}Mn_{0.9})O$	4.508	Mn^{2+}: 0.67 Ni^{2+}: 0.69	Mn^{2+}	MnO: 1051 NiO: 1738	843 1188	Mn^{2+}	MnO: 2884 NiO: 3836	2077 2809	0.00	0.53
$(Co_{0.001}Sr_{0.999})O$	5.282	Sr^{2+}: 1.16 Co^{2+}: 0.74	Sr^{2+}	SrO: 704 CoO: 1447	571 1101	Sr^{2+}	SrO: 1872 CoO: 2908	1450 2604	1.19	1.27
$(Fe_{0.001}Sr_{0.999})O$	5.282	Sr^{2+}: 1.16 Fe^{2+}: 0.77	Sr^{2+}	SrO: 704 FeO: 1383	571 997	Sr^{2+}	SrO: 1872 FeO: 2818	1450 3087	0.64	1.12
$(Ni_{0.001}Sr_{0.999})O$	5.281	Sr^{2+}: 1.16 Ni^{2+}: 0.69	Sr^{2+}	SrO: 704 NiO: 1480	571 1188	Sr^{2+}	SrO: 1872 NiO: 2955	1450 2809	1.48	1.42

†a is the equilibrium lattice parameter of the solution, r is the cation radius,[30] γ^* is the unrelaxed surface energy of the oxide at the lattice parameter of the solution, γ is the relaxed surface energy of the oxide, $E_{elastic}$ is the elastic energy[31] of the misfitting impurity in the bulk environment, and ΔE_{bond} is the approximate difference between the cation–anion bond energies[28] of the oxides.

dominated by surface energy effects, which increases the driving force for subsurface segregation. For example, a larger cation covering the surface layer might increase the propensity for the smaller cation to occupy the layer below the surface.

Strong oscillatory subsurface segregation might have a significant effect on spatially averaged experimental measurements of surface concentration. For example, the measured concentration at a surface with a solute distribution like those in Fig. 2 might vary considerably depending on the resolution of the measurement technique.

V. Conclusions

Segregation of isovalent solute cations to (001) and (011) free surfaces in metal oxides has been studied using free energy minimization. Conventional pair potentials are used to describe atomic interactions. The local harmonic approximation is employed to approximate the vibrational energy, and the mean-field effective atom method to simulate a solid solution.

Surface energy effects are found to dominate segregation behavior when in competition with misfit strain effects. Solute misfit effects appear to drive segregation to subsurface atomic layers.

Langmuir–McLean calculations of solute concentrations at free surfaces are found to agree satisfactorily with FEM results. This suggests that vibrational effects are of limited importance in determining segregation to a free surface in these systems. However, segregation to subsurface atomic layers is found to be appreciable, and the classical Langmuir–McLean approach is usually limited to the single surface atomic plane.

References

[1]W. C. Johnson, "Grain Boundary Segregation in Ceramics," *Metall. Trans. A*, **8A**, 1413–22 (1977).

[2]A. Roshko and W. D. Kingery, "Segregation to Special Boundaries in MgO," *J. Am. Ceram. Soc.*, **68**, C-331–C-333 (1985).

[3]S. Baik and C. L. White, "Anisotropic Calcium Segregation to the Surface of Al_2O_3," *J. Am. Ceram. Soc.*, **70**, 682–88 (1987).

[4]P. W. Tasker, E. A. Colbourn, and W. C. Mackrodt, "Segregation of Isovalent Impurity Cations at the Surface of MgO and CaO," *J. Am. Ceram. Soc.*, **68**, 74–80 (1985).

[5]S. M. Foiles, "Calculation of the Surface Segregation of Ni–Cu Alloys with the Use of the Embedded-Atom Method," *Phys. Rev. B*, **32**, 7685–93 (1985).

[6]W. C. Mackrodt and P. W. Tasker, "Segregation Isotherms at the Surfaces of Oxides," *J. Am. Ceram. Soc.*, **72**, 1576–83 (1989).

[7]S. M. Foiles, "Calculation of Grain-Boundary Segregation in Ni–Cu Alloys," *Phys. Rev. B*, **40**, 11502–506 (1989).

[8]R. LeSar, R. Najafabadi, and D. J. Srolovitz, "Finite-Temperature Defect Properties from Free-Energy Minimization," *Phys. Rev. Lett.*, **63**, 624–27 (1989).

[9]A. P. Sutton, "Temperature-Dependent Interatomic Forces," *Philos. Mag. A*, **60**, 147–59 (1989).

[10]R. Najafabadi, H. Y. Wang, D. J. Srolovitz, and R. LeSar, "A New Method for the Simulation of Alloys: Application to Interfacial Segregation," *Acta Metall.*, **39**, 3071–82 (1991).

[11]H. Y. Wang, R. Najafabadi, D. J. Srolovitz, and R. LeSar, "Segregation to and Structure of [001] Twist Grain Boundaries in Cu–Ni Alloys," *Acta Metall.*, **41**, 2533–46 (1993).

[12]L. Zhao, R. Najafabadi, and D. J. Srolovitz, "Finite Temperature Vacancy Formation Thermodynamics: Local Harmonic and Quasi-Harmonic," *Model. Simul. Mater. Sci.*, **1**, 539–51 (1993).

[13]C. Battaile, R. Najafabadi, and D. J. Srolovitz, "Simulation of Segregation to Interfaces in Metal Oxides"; pp. 435–40 in Materials Research Society Symposia Proceedings, Vol. 357, *Structure and Properties of Interfaces in Ceramics*. Edited by D. Bonnell, M. Rühle, and U. Chowdhry. Materials Research Society, Pittsburgh, PA, 1995.

[14]E. A. Colbourn, W. C. Mackrodt, and P. W. Tasker, "The Segregation of Calcium Ions at the Surface of Magnesium Oxide," *J. Mater. Sci.*, **18**, 1917–24 (1983).

[15]W. C. Mackrodt, "Atom Lattice Simulations of the Structure, Energetics, and Impurity Segregation Behaviour of Ceramic Boundaries," *Mater. Sci. Res.*, **21**, 271–80 (1987).

[16]L. V. Woodcock and K. Singer, "Thermodynamic and Structural Properties of Liquid Ionic Salts Obtained by Monte Carlo Computation," *Trans. Faraday Soc.*, **67**, 12–30 (1970).

[17]M. J. Norgett, "A Born Model Calculation of the Energies of Vacancies, Ion Interstitials, and Inert Gas Atoms in Calcium Flouride," *J. Phys. C*, **4**, 298–306 (1971).

[18]T. S. Chen, F. W. de Wette, and G. P. Alldredge, "Studies of Vibrational Surface Modes in Ionic Crystals. I. Detailed Shell-Model Studies for the Unrelaxed (001) Face of Seven Crystals Having the Rocksalt Structure," *Phys. Rev. B*, **15**, 1167–86 (1977).

[19]N. Anastasiou and D. Fincham, "Programs for the Dynamic Simulations of Liquids and Solids II. MDIONS: Rigid Ions Using the Ewald Sum," *Comput. Phys. Commun.*, **25**, 159–76 (1982).

[20]C. R. A. Catlow and W. C. Mackrodt (Eds.), *Computer Simulation of Solids*. Springer-Verlag, Berlin, Federal Republic of Germany, 1982.

[21]A. Jockisch, U. Schröder, F. W. de Wette, and W. Kress, "Relaxation and Dynamics of the (110) Surface of the Cesium Chloride Structure Crystals CsCl, CsBr, and CsI," *Surf. Sci.*, **297**, 245–51 (1993).

[22]P. P. Ewald, "Die Berechnung Optischer und Elektrostatischer Gitterpotentiale," *Ann. Phys. (Leipzig)*, **64**, 253–87 (1921).

[23]D. C. Wallace, *Thermodynamics of Crystals*; pp. 265–71. Wiley, Sydney, Australia, 1972.

[24]B. G. Dick and A. W. Overhauser, "Theory of the Dielectric Constants of Alkali Halide Crystals," *Phys. Rev.*, **112**, 90–103 (1958).

[25]P. A. Mulheran, "Structural Calculations of Oxide Surfaces at Finite Temperature," *Philos. Mag. A*, **68**, 799–808 (1993).

[26]C. Battaile, R. Najafabadi, and D. J. Srolovitz; unpublished results.

[27]S. Nambu and M. Oiji, "A Microscopic Calculation of Thermal Properties of Ionic Solid Solutions"; pp. 915–18 in *Computer Aided Innovation of New Materials*. Edited by M. Doyama *et al.* Elsevier, New York, 1991.

[28]M. J. L. Sangster and A. M. Stoneham, "Calculations of Off-Centre Displacements of Divalent Substitutional Ions in CaO, SrO, and BaO from Model Potentials," *Philos. Mag. B*, **43**, 597–608 (1981).

[29]W. H. Press, *et al.*, *Numerical Recipes in C: The Art of Scientific Computing*, 2nd ed.; pp. 420–25. Cambridge University Press, New York, 1992.

[30]W. D. Kingery, H. K. Bowen, and D. R. Uhlmann, *Introduction to Ceramics*, 2nd ed.; p. 58. Wiley, New York, 1976.

[31]J. Friedel, "Electronic Structure of Primary Solid Solutions in Metals," *Adv. Phys.*, **3**, 446–507 (1954). □